Controlling coverage of solution cast materials with unfavourable surface interactions

V. M. Burlakov, G. E. Eperon, H. J. Snaith, S. J. Chapman, and A. Goriely

Citation: Applied Physics Letters **104**, 091602 (2014); doi: 10.1063/1.4867263
View online: http://dx.doi.org/10.1063/1.4867263
View Table of Contents: http://scitation.aip.org/content/aip/journal/apl/104/9?ver=pdfcov
Published by the AIP Publishing

Controlling coverage of solution cast materials with unfavourable surface interactions

V. M. Burlakov,[1] G. E. Eperon,[2] H. J. Snaith,[2] S. J. Chapman,[1] and A. Goriely[1]
[1]*Mathematical Institute, University of Oxford, Woodstock Rd, Oxford OX2 6GG, United Kingdom*
[2]*Clarendon Laboratory, Department of Physics, University of Oxford, Parks Road, Oxford OX1 3PU, United Kingdom*

(Received 8 November 2013; accepted 18 February 2014; published online 3 March 2014)

Creating uniform coatings of a solution-cast material is of central importance to a broad range of applications. Here, a robust and generic theoretical framework for calculating surface coverage by a solid film of material de-wetting a substrate is presented. Using experimental data from semiconductor thin films as an example, we calculate surface coverage for a wide range of annealing temperatures and film thicknesses. The model generally predicts that for each value of the annealing temperature there is a range of film thicknesses leading to poor surface coverage. The model accurately reproduces solution-cast thin film coverage for organometal halide perovskites, key modern photovoltaic materials, and identifies processing windows for both high and low levels of surface coverage. © *2014 AIP Publishing LLC*. [http://dx.doi.org/10.1063/1.4867263]

There is a broad family of emerging photovoltaics which rely on the processing of uniform thin-films of (poly)crystalline semiconductors from solutions. Such thin films are often thermodynamically unstable and upon post-annealing they tend to partially de-wet the substrate by the growth of pinholes, which may grow further and even break the film into islands (see Ref. 1, and the references therein). The driving force for de-wetting is the minimization of the total energy of the film, the substrate, and of the film-substrate interface. The initial stage of hole nucleation and de-wetting may happen via several mechanisms, both in liquid state during film deposition[2] and at the beginning of the annealing process where temperature can accelerate the growth of holes.[3] Hole nucleation during film fabrication can be controlled by carefully selecting the solvent and its evaporation rate.[4,5] However, the multiple mechanisms of hole nucleation during annealing are less controllable, since most of them are due to largely inevitable imperfections in the film or film-substrate interface structures.

The main process decreasing surface coverage of the film during annealing is the growth of holes. Simple models of an isolated cylindrical hole show that it will grow further or collapse depending on the value of its radius relative to some critical value.[3] In the complex environment of real films, there are many holes of various sizes that interact with each other by changing the film thickness or the distribution of elastic stress over the film. Moreover, the annealing process is meant to improve the functional properties of the film by removing solvent residues and excess non-stoichiometric volatile components and by improving its crystalline structure. These changes also contribute to possible variations in film thickness and composition during annealing, which further influences the evolution of the holes. While the theoretical description of individual hole growth is well developed,[6] little is known on the simultaneous evolution of multiple holes and their cumulative influence on the surface coverage apart from the dilute case where hole-hole interactions can be decoupled.[7,8] In this Letter, we also use the dilute assumption to present a robust semi-analytical model, which provides an understanding of the key parameters helping to control and maximize surface coverage by thin films. The model is applied to the photovoltaic material $CH_3NH_3PbI_{3-x}Cl_x$.

A recent breakthrough in emerging photovoltaics, which has enabled the power conversion efficiency of cells to move beyond 15%,[9–13] has taken place in large part due to a novel organic-inorganic compound with perovskite-type crystal structure.[14] A solution-processed organolead halide perovskite, $CH_3NH_3PbI_{3-x}Cl_x$, is not only an effective photovoltaic sensitizer but can also play the role of an electron transporter when formed from solution within an inert mesoporous alumina scaffold.[11] This property enables minimisation of energy losses and a correspondingly high open-circuit voltage of 1.1 V. Subsequent thickness reduction and removal of the mesoporous inert scaffold results in an increase in the photocurrent of the solar cell.[10] However, the formation of a uniform solid thin film of the perovskite absorber without the assistance of the mesoporous scaffold cannot be easily realized. In the standard solution-processing technique used to form these films, a non-stoichiometric precursor is spin-coated on a substrate and undergoes subsequent annealing to form the crystalline perovskite. During this annealing, solvent evaporation and stoichiometry-driven mass loss contribute to the formation of holes within the final crystalline layer. Characteristic SEM images of two films of this perovskite deposited by spin-coating on a smooth amorphous TiO_2 surface coated upon a c-Si wafer are shown in Fig. 1. As-deposited films obtained after solvent drying but before annealing (a) and (c) look rather smooth. After annealing at 100 °C for 60 min, a granular structure is observed due to hole growth (darker areas in (b) and (d)). Note also that the average hole diameter is much larger for thicker films. From this initial observation and the fact that there is 10%–15% volume loss during annealing, we have developed a model describing the annealing-induced evolution of surface coverage by thin films.

The model is based on a few basic assumptions: (i) all holes have cylindrical shape and never impinge upon each other; (ii) the holes are nucleated either before or shortly after annealing starts and nucleation does not take place during

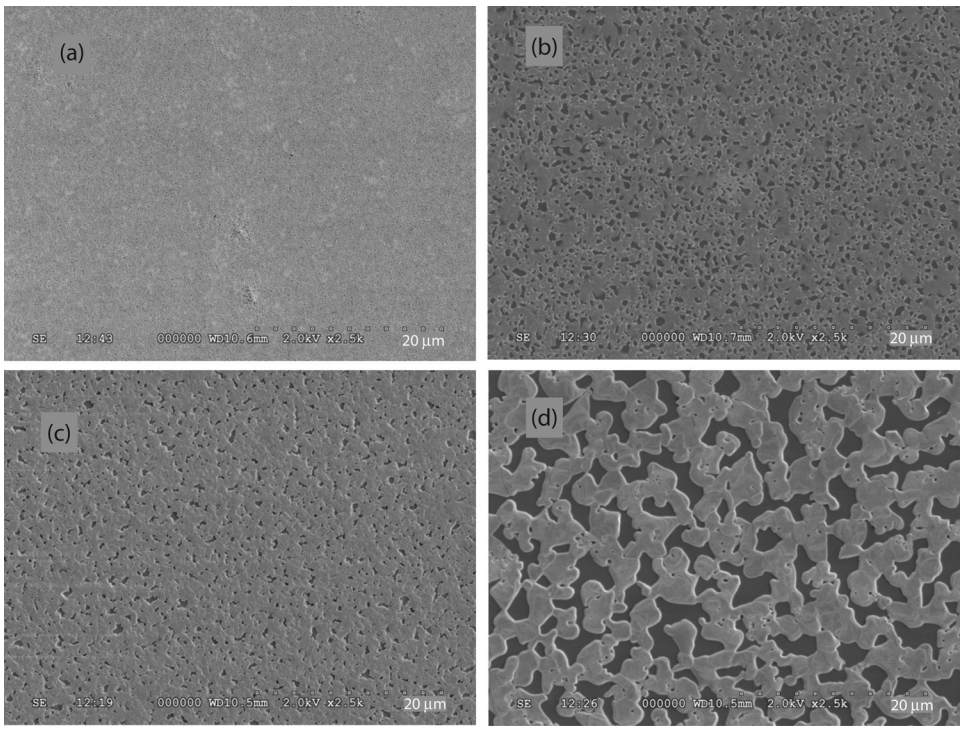

FIG. 1. SEM images of two films of $CH_3NH_3PbI_{3-x}Cl_x$ on smooth amorphous TiO_2-coated silicon substrate. (a) As deposited thin (~50 nm) film; (b) thin film annealed for 1 h at 100 C; (c) as deposited thick (~250 nm) film; (d) thick film annealed for 1 h at 100 C. Film thicknesses (averaged over the covered area) after annealing are 10%–20% lower than those before annealing.

the hole growth/shrinkage process; (iii) elastic stresses in the film are fully relaxed before noticeable change in film morphology takes place, (iv) no discrimination is made between solvent loss, and driven-off non stoichiometric components, since they are de-facto volatile, and we use the generic term "solvent" to describe all mass loss. Then, the surface and interface energy, E, of a film containing N cylindrical holes and sitting on a substrate with the area $L \times L$ is given by

$$E = \gamma_F \left(2\pi h \sum_{k=1}^{N} R_k + L^2 - \pi \sum_{k=1}^{N} R_k^2 \right) + \gamma_I \left(L^2 - \pi \sum_{k=1}^{N} R_k^2 \right) + \gamma_S \pi \sum_{k=1}^{N} R_k^2, \quad (1)$$

where h is the film thickness; γ_F, γ_S, and γ_I are surface energies of film, substrate, and the film-substrate interface energy, respectively; and R_i are the radii of the holes. Assuming a gradient flow of energy, the time evolution of holes radii is given by

$$\frac{dR_i}{dt} = -\Gamma \frac{dE}{dR_i} = -2\pi\Gamma(\gamma_F h - R_i(\gamma_F + \gamma_{IS})), \quad (2)$$

where $\gamma_{IS} = \gamma_I - \gamma_S$ and Γ is the kinetic coefficient which depends on the particular physical mechanisms of material flow. To account for the presence of solvent in the film, we may represent the kinetic coefficient as consisting of two components, $\Gamma = \Gamma_0(n_0 - \bar{n}) + \Gamma_1 \bar{n}$, with Γ_0 accounting for pure material flow and Γ_1 accounting for that mediated by the solvent, which has an average concentration of $\bar{n}$ and a maximum concentration of n_0. At typical temperatures used for annealing (~100 °C), the pure film material does not flow. Therefore, we assume that the holes change size only due to the presence of solvent, i.e., $\Gamma \approx \Gamma_1 \bar{n}$, and (2) takes the form

$$\frac{dR_i}{dt} = A_{FL} \bar{n} (R_i - R_C), \quad (3)$$

where $A_{FL} = 2\pi\Gamma_1(\gamma_F + \gamma_{IS})$ is the material flow rate per unit solvent concentration, and $R_C = h(t)/(1 + \gamma_{IS}/\gamma_F)$ is a time-dependent critical radius for hole growth. With solvent evaporation, the film volume changes according to the equation

$$\frac{dV}{dt} = -A_{EV} n_s a^3 L^2, \quad (4)$$

where $n_s = n(h,t)$ is the solvent concentration at the film surface, a^3 is an average molecular volume in the film material, and $A_{EV} n_s$ is the molecular evaporation rate per unit surface area. Here, we neglect solvent evaporation from the side walls of the holes and the change in the film area due to the holes, i.e., we consider the high coverage limit, expressed by the condition

$$\frac{1}{L^2} \pi \sum_{i=1}^{N} R_i^2 \ll 1. \quad (5)$$

To close the system, we express the concentration at the surface n_s in terms of the average volume fraction $\bar{n}$. The solvent concentration inside the film is described by

$$\frac{\partial n}{\partial t} = D \frac{\partial^2 n}{\partial z^2}, \quad 0 < z < h, \quad (6)$$

$$D \frac{\partial n}{\partial z} = 0 \quad \text{on} \quad z = 0, \quad (7)$$

$$D \frac{\partial n}{\partial z} = -A_{EV}\, n \quad \text{on} \quad z = h, \quad (8)$$

where D is the temperature dependent diffusion coefficient for the solvent. In the case of slow evaporation

($\Pi \equiv hA_{EV}/D \ll 1$), the evolution is quasistatic, the concentration profile across the film is close to quadratic, and it can be shown that n_s and $\bar{n}$ are related by

$$\bar{n} \approx \left(1 + \frac{hA_{EV}}{3D}\right) n_s. \tag{9}$$

Under the approximation (9), the average concentration evolves according to

$$\frac{d\bar{n}}{dt} = -\frac{A_{EV}}{h} n_s \approx -\frac{\bar{n}A_{EV}}{h(1 + hA_{EV}/3D)}. \tag{10}$$

If the thickness h is assumed to vary slowly with time, it can be assumed constant with respect to the typical time scale for the variation of n so that the solution for $n = n(t)$ is $\bar{n}(t) = \bar{n}(0)e^{-\beta t}$, where $\beta = A_{EV}\left(h + h^2 A_{EV}/3D\right)^{-1}$. The validity of the approximation (9) can be assessed by comparing this expression with the actual decay of $\bar{n}$. The results, presented in Fig. 2, show that the approximation is good even when Π is as large as 10.

Within the approximations given by (5) and (9), it is possible to study the film coverage as a function of the film thickness. Dividing (3) by (4) and using (9) and $V = hL^2$ gives

$$\frac{dR_i}{dh} = -\frac{A_{FL}}{a^3 A_{EV}} \left(R_i - \frac{h}{1 + \gamma_{IS}/\gamma_F}\right)\left(1 + \frac{hA_{EV}}{3D}\right), \tag{11}$$

with solution

$$R_i(h) = R_i^*(h) + \left[R_i(h_0) - R_i^*(h_0)\right] e^{-c_0(h-h_0) - c_1(h^2 - h_0^2)}, \tag{12}$$

where

$$c_0 = \frac{A_{FL}}{a^3 A_{EV}}, \quad c_1 = \frac{A_{FL}}{6a^3 D}, \quad c_2 = 1/(1 + \gamma_{IS}/\gamma_F),$$

$$R^*(h) = c_2 h - \frac{c_2}{\sqrt{c_1}} F\left(\frac{c_0}{2\sqrt{c_1}} + \sqrt{c_1} h\right),$$

$$F(\xi) = e^{-\xi^2} \int_0^{\xi} e^{\eta^2}\, d\eta.$$

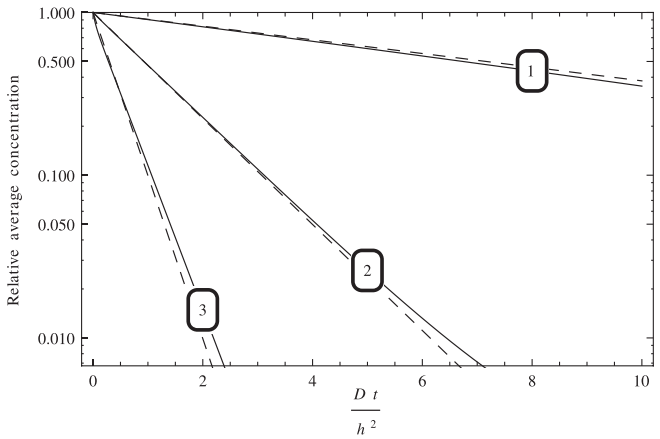

FIG. 2. Simulated time evolution of the average solvent concentration during its evaporation from one side of a film of constant thickness h (solid lines) compared to the simplex exponential approximation (10) (dashed lines) for $\Pi = 0.1$ (1), 1 (2), and 10 (3).

This solution implies that the hole size distribution remains Gaussian, if it was initially Gaussian. Indeed, starting with an initial Gaussian distribution $f_0(R) = Z^{-1}\exp(-(R-R_0)^2/2\sigma^2)$ and writing $R(h_0)$ in terms of $R(h)$ leads to a final Gaussian distribution

$$f_\alpha(R) = Z_1^{-1}\exp(-(R - R_1)^2/2\sigma_1^2),$$
$$R_1 = R^*(h) + \alpha(R_0 - R^*(h_0)), \quad \sigma_1 = \alpha\sigma, \tag{13}$$

where $\ln\alpha = c_0(h_0 - h) + c_1(h_0^2 - h^2)$. The Gaussian distribution (13) has a shifted peak position R_1 and a renormalized width σ_1. We use here a single Gaussian distribution, but the self-similarity of the distribution of hole sizes is also applicable to the more generic case when the initial distribution is represented by a sum of Gaussians.

Using (13) and taking a volume loss of 10% such that $h = 0.9h_0$, we can now readily compute the surface coverage $C(h_0, T)$ as a function of the initial film thickness h_0 and the annealing temperature T without the need to perform expensive simulations of the evolution of multiple holes. First, we determined experimentally the distribution of hole sizes before annealing from SEM images of $CH_3NH_3PbI_{3-x}Cl_x$ films deposited on smooth TiO_2 substrates shown in Figs. 1(a) and 1(c) using the software ImageJ.[15] Typically, this experimental distribution (see Fig. 3) is characterized by many holes assigned the same size and can be approximated by a Gaussian of the form $f_0(R) = Z^{-1}\exp(-(R-R_0)^2/2\sigma^2)$ with $R_0 = 115$ nm and $\sigma = 125$ nm.

This Gaussian then evolves to that given in (13) under annealing, which is used to determine the film coverage as a function of the parameter α via

$$C(\alpha) = 1 - \frac{1}{L^2}\int R^2 f_\alpha(R)\, dR = 1 - (1 - C_0)\frac{\int R^2 f_\alpha(R)\, dR}{\int R^2 f_0(R)\, dR}, \tag{14}$$

where C_0 is the film coverage before annealing, which we take to be 90%. As the value of γ_{IS}/γ_F is unknown, we considered several values from the range $(-1, 1)$ and selected $\gamma_{IS}/\gamma_F = 0.54$ as the best fit to experimental data.[16] We now

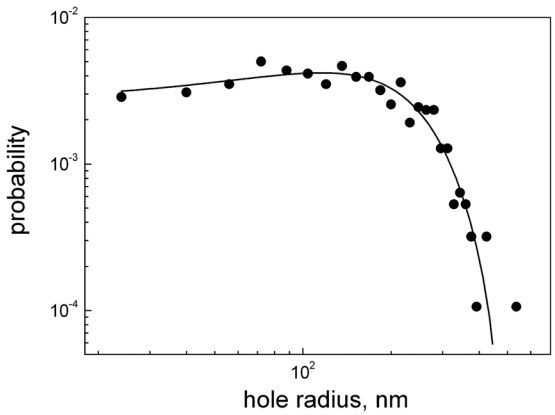

FIG. 3. Distribution of hole radii (symbols) before annealing obtained by averaging over 10 samples of thicknesses 200–600 nm. Solid line shows Gaussian distribution with the parameters $R_0 = 115$ nm and $\sigma = 125$ nm.

fit $C(\alpha)$ to three experimental data points using the least squares method to determine the parameter values $c_0 = 40.10\ \mu\text{m}^{-1}$ and $c_1 = 15.17\ \mu\text{m}^{-2}$ for a given annealing temperature $T = 100\,^{\circ}\text{C} = 0.032$ eV. Note that the ratio $c_1/c_0 = A_{EV}/6D = 0.378\ \mu\text{m}^{-1}$ gives the value of $\Pi = hA_{EV}/D = 2.27$ (for $h = 1\ \mu$m), for which the approximation (9) is good.

The next step in calculating $C(h_0, T)$ is to obtain the temperature dependence of c_0 and c_1. These can be written in the form

$$c_0(T) = c_{00} \exp\left(-\frac{E_{FL} - E_{EV}}{k_B T}\right), \tag{15a}$$

$$c_1(T) = c_{10} \exp\left(-\frac{E_{FL} - E_{DI}}{k_B T}\right), \tag{15b}$$

where c_{00} and c_{10} are constant, and E_{FL}, E_{EV}, and E_{DI} are activation energies for material flow, solvent evaporation, and solvent diffusion, respectively. The difference in activation energies is obtained fitting to additional experimental data related to film annealing at 85 °C and 120 °C and is found to be $E_{FL} - E_{EV} = 0.02274$ eV, $E_{FL} - E_{DI} = 0.02270$ eV. Once the four parameters c_{00}, c_{10}, $E_{FL} - E_{EV}$ and $E_{FL} - E_{DI}$ entering (14) are known, we can contour plot $C(h_0, T)$ as shown in Fig. 4. According to this model, at a given annealing temperature, the coverage first decreases with increasing initial film thickness and then increases, reaching the highest levels with the thickest films and the lowest annealing temperatures. In particular, for an annealing temperature suitable for crystallization of the compound $CH_3NH_3PbI_{3-x}Cl_x$ ($\sim 100\,^{\circ}$C (Ref. 11)), our model suggests that it would be difficult to achieve coverage higher than 70% for films thinner than 500 nm. To obtain coverage over 85%, the film must be either much thicker (>900 nm) or much thinner (<50 nm). The latter, however, is difficult to manufacture with reasonably high initial coverage. This non-monotonic behaviour for surface coverage during annealing is due to the combined effect of solvent evaporation, the growth of holes, and film thickness. For thinner films (<100 nm), the critical radius is low and the majority of holes have size above critical and grow during annealing. At the same time, the decrease in solvent concentration due to evaporation is so rapid that there is no time for these holes to grow large, and the surface coverage is mostly accounted for by a large number of small holes (Fig. 1(b)) which remains close to the initial value (90%). For thicker films (>600 nm), the critical radius is so large that only a minority of holes are larger. The decrease in surface coverage associated with the growth of these holes is overcompensated by its increase due to majority of shrinking holes, which makes the overall coverage high. The evolution of surface coverage for films with intermediate thicknesses is dominated by a significant number of holes growing to relatively large sizes (Fig. 1(d)) resulting in an overall decrease of surface coverage during annealing relative to its initial value.

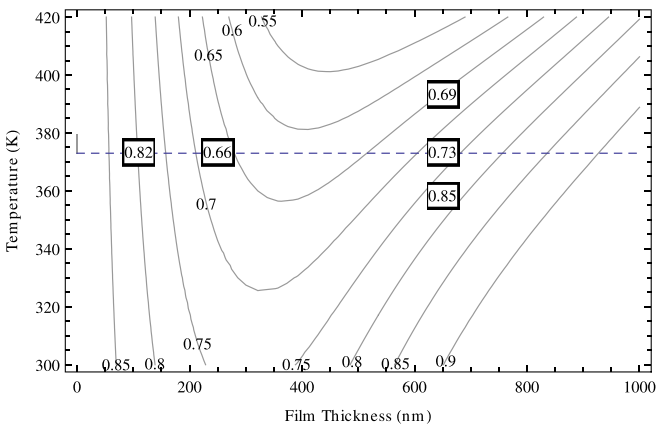

FIG. 4. Contour plot of surface coverage as a function of initial film thickness and annealing temperature calculated using (14) with the initial hole size distribution given in Fig. 3 and $\gamma_{IS}/\gamma_F = 0.15$. The horizontal dotted line marks the annealing temperature of 100 °C suitable for crystallisation of $CH_3NH_3PbI_{3-x}Cl_x$. Values in squares indicate the corresponding experimental values of coverage used in the fitting procedure.

The main result of our study illustrated in Fig. 4 was obtained using a particular distribution (Gaussian) of initial hole size, which is conserved during the entire annealing process through neglecting the effect of hole impingement. This raises the question of the dependence of the contour plot in Fig. 4 upon the initial hole size distribution and upon hole impingement. Our model calculations show that the shape of the contour plot in Fig. 4 is mostly unchanged, when the initial hole size distribution is approximated by a different Gaussian.[16] Such stability of the contour plot is due to the fact that the final coverage is calculated self-consistently, i.e., we use a few experimental values of surface coverage to obtain the model parameters, which then are used to calculate surface coverage in a wider range of (h_0, T) parameter space.

Hole impingement, if significant, would modify (3) and could significantly change the shape of the contour plot in Fig. 4. The impact of hole impingement can be estimated by analysing the value of the holes impingement factor (HIF) defined as $\text{HIF} = \langle l \rangle^{-1} \langle dR/dt \rangle \tau_{ev}$, where $\langle l \rangle$ is the average hole separation, $\langle dR/dt \rangle$ is the average hole growth rate given by (3), and $\tau_{ev} = \beta^{-1} = (1 + \Pi/3)h/A_{ev}$ is a characteristic solvent evaporation time, and hence a characteristic time available for hole growth (see supplementary material for details). For the parameter values obtained in our analysis and used for creating the contour plot in Fig. 4, the value of HIF is found not to exceed 0.1, which indicates that hole impingement effects are of minor importance. This means that the accuracy of our contour plot in Fig. 4 is mainly determined by the accuracy of the experimental data on which it is built.

In summary, we have presented a robust and generic theoretical model to quantify the effect of the main parameters on surface coverage by thin solid films exhibiting solvent loss and having an unfavourable film-substrate interaction during annealing. Our analysis shows that even without changing the adhesive properties of the substrate, which could limit substrate choice or electronic optimisation, the surface coverage can be substantially increased by tuning film thickness and decreasing the annealing temperature. The latter, when applied to $CH_3NH_3PbI_{3-x}Cl_x$ films, results in an average increase in the surface coverage to over 85% as demonstrated in recent experiments.[17,18] Hence, by careful control and optimisation of processing parameter space (thickness, temperature, solvent, evaporation rate, and deposition method), it is feasible to obtain much higher surface

coverage and eventual good operation of solution-cast thin film optoelectronic devices.

The authors thank Colin Please, Cameron Hall, Giles Richardson, and Jamie Foster for fruitful discussions. This work was supported by EPSRC and Oxford Photovoltaics Ltd., through a Nanotechnology KTN CASE award, the European Research Council (ERC) HYPER PROJECT No. 279881. This publication is based in part upon work supported by Award No. KUK-C1-013-04, made by King Abdullah University of Science and Technology (KAUST). A.G. is a Wolfson/Royal Society Merit Award Holder and acknowledges support from a Reintegration Grant under EC Framework VII. V.M.B. is an Oxford Martin School Fellow and this work was in part supported by the Oxford Martin School. S.J.C. and A.G. acknowledge support from EPSRC Award No. EP/I017070/1.

[1]C. V. Thompson, Annu. Rev. Mater. Res. **42**, 399 (2012).
[2]J. Bischof, D. Scherer, S. Herminghaus, and P. Leiderer, Phys. Rev. Lett. **77**, 1536 (1996).
[3]D. J. Srolovitz and M. G. Goldiner, JOM **47**, 31 (1995).
[4]T. G. Stange, R. Mathew, D. F. Evans, and W. A. Hendrickson, Langmuir **8**, 920 (1992).
[5]C. W. Extrand, Langmuir **9**, 475 (1993).
[6]D. J. Srolovitz and S. A. Safran, J. Appl. Phys. **60**, 255 (1986).
[7]I. Botiz, P. Freyberg, N. Stingelin, A. C.-M. Yang, and G. Reiter, Macromolecules **46**, 2352 (2013).
[8]G. Reiter, Phys. Rev. Lett. **68**, 75 (1992).
[9]H.-S. Kim, C.-R. Lee, J.-H. Im, K.-B. Lee, T. Moehl, A. Marchioro, S.-J. Moon, R. Humphry-Baker, J.-H. Yum, J. E. Moser, M. Gratzel, and N.-G. Park, Sci. Rep. **2**, 591 (2012).
[10]J. M. Ball, M. M. Lee, A. Hey, and H. J. Snaith, Energy Environ. Sci. **6**, 1739 (2013).
[11]M. M. Lee, J. Teuscher, T. Miyasaka, T. N. Murakami, and H. J. Snaith, Science **338**, 643 (2012).
[12]J. Burschka, N. Pellet, S.-J. Moon, R. Humphry-Baker, P. Gao, M. K. Nazeeruddin, and M. Gratzel, Nature **499**, 316 (2013).
[13]M. Liu, M. B. Johnston, and H. J. Snaith, Nature **501**, 395 (2013).
[14]A. Kojima, K. Teshima, Y. Shirai, and T. Miyasaka, J. Am. Chem. Soc. **131**, 6050 (2009).
[15]M. D. Abramoff, P. J. Magalhaes, and S. J. Ram, Biophotonics Int. **11**, 36 (2004).
[16]See supplementary material at http://dx.doi.org/10.1063/1.4867263 for details.
[17]G. E. Eperon, V. M. Burlakov, P. Docampo, A. Goriely, and H. J. Snaith, Adv. Funct. Mater. **24**, 151 (2014).
[18]G. E. Eperon, V. M. Burlakov, A. Goriely, and H. J. Snaith, ACS Nano **8**, 591 (2014).